

Hydrodynamic interactions between a sedimenting squirmer and a planar wall

Henry Shum¹, D. Palaniappan² and Y.-N. Young³†

¹Department of Mathematics, University of Waterloo, Waterloo, ON N2J 3G1, Canada

²Department of Mathematics and Statistics, Texas A&M University - Corpus Christi, TX 78412, USA

³Department of Mathematical Sciences, New Jersey Institute of Technology, Newark, NJ, 07102, USA

(Received xx; revised xx; accepted xx)

The hydrodynamic interactions between a sedimenting microswimmer and a solid wall have ubiquitous biological and technological applications. A plethora of gravity-induced swimming dynamics near a planar no-slip wall provides a platform for designing artificial microswimmers that can generate directed propulsion through their translation-rotation coupling near a wall. In this work we provide exact solutions for a squirmer (a model swimmer of spherical shape with a prescribed slip velocity) facing either towards or away from a planar wall perpendicular to gravity. These exact solutions are used to validate a numerical code based on the boundary integral method with an adaptive mesh for distances from the wall down to 0.1% of the squirmer radius. This boundary integral code is then used to investigate the rich gravity-induced dynamics near a wall, mapping out the detailed bifurcation structures of the swimming dynamics in terms of orientation and distance to the wall. Simulation results show that a squirmer may transverse along the wall, move to a fixed point at a given height with a fixed orientation in a monotonic way or in an oscillatory fashion, or oscillate in a limit cycle in the presence of wall repulsion.

1. Introduction

Microswimmers behave very differently near a wall as their interactions with a solid boundary alter their speed, direction, and how they interact with each other (Shum *et al.* 2010; Takagi *et al.* 2014; Elgeti & Gompper 2016), giving rise to many interesting phenomena, such as the swirling of bacteria next to a substrate and clustering of phoretic Janus particles and bacteria near a wall. While the far-field flow attracts and aligns a pusher (puller) to move along (normal to) a no-slip wall, near-field hydrodynamics, steric interactions and contact dynamics give rise to wall scattering with the swimmer escaping from the wall at a characteristic angle that is independent of the initial direction of approach to the wall (Berke *et al.* 2008; Li & Tang 2009).

The hydrodynamic interactions between a microswimmer and a solid wall are more complex when the swimmer sediments to the wall under gravity (due to the density mismatch between the swimmer and the surrounding fluid). Several types of dynamics of a sedimenting swimmer have been reported: scattering (escaping) from the wall, swimming along the wall at a fixed distance and tilted orientation, and periodic bouncing on the wall (Or & Murray 2009; Crowley & Or 2010). Under gravity, artificial surface walkers or micro rollers stay close to the wall. At the same time, they rotate under an external force field, exploiting their interactions with a solid surface to generate directed propulsion (Tierno *et al.* 2008; Sing *et al.* 2010; Driscoll *et al.* 2017). These microswimmers are easy to manipulate for directed transport and offer wide applications in targeted therapeutics and microsurgery (Alapan *et al.* 2020; Ahmed *et al.* 2021).

The interactions between a flagellated swimmer and a flat solid wall have been modeled using

† Email address for correspondence: yyoung@njit.edu

a multipole approach (Spagnolie & Lauga 2012), which is shown to give good agreement with boundary integral simulations. Through the contribution of each singularity to the effect of a wall on the flagellated swimmer, the reduced model captures the main dynamic features of the wall-induced hydrodynamics of a microswimmer. Alternatively, a microswimmer is often simplified and modeled as a squirming sphere with a slip velocity on the surface to mimic the surrounding flow created by the layer of beating cilia on the microswimmer (Lighthill 1952; Blake 1971*b*). Such simplification allows the usage of the Lorentz reciprocal theorem to derive an exact solution for a squirming sphere close to a no-slip surface (Papavassiliou & Alexander 2017). Exact solutions for a sphere moving towards or away from a flat wall have been derived by Brenner (1961). Cox & Brenner (1967) later derived the near-field solution that shows the asymptotic divergence of the viscous drag coefficient as the sphere approaches the solid wall. For a squirmer interacting with a solid wall through the hydrodynamic interactions, Théry *et al.* (2023) combined the far-field flow of a sedimenting sphere (Kim & Karrila 2013) with the squirming flow to illustrate the different swimming dynamics near a wall and noted that the far-field approximation may not be uniformly valid across different types of squirmer dynamics. For example, oscillatory (bouncing) dynamics of a squirmer may involve motion both near to and far from the wall, and the sliding squirmer can also occur in the near-field (Li & Ardekani 2014; Rühle *et al.* 2018; Kuhr *et al.* 2019).

In this work we seek to elucidate the detailed swimming dynamics of a single squirmer sedimenting toward a flat wall, using a boundary integral code validated for both the near-field and far-field hydrodynamics. In particular, we seek to quantify how the swimming dynamics of a squirmer sedimenting to a wall depends on α (the ratio of sedimenting velocity to swimming speed) and β (the ratio of the first two squirming mode amplitudes). We first derive exact solution for a squirming sphere sedimenting towards a flat no-slip wall, using the approach in Brenner (1961). We use this analytic solution to validate a boundary integral code, which is highly efficient and accurate for us to examine the dynamics of a sedimenting squirmer near a flat wall over a wide range of parameters.

This paper is organized as follows. In § 2 we present the formulation for a squirmer under gravity in the presence of a planar bottom wall. We assume the squirmer is immersed in a viscous Stokes flow, and there may be a steric repulsion between the solid wall and the squirmer when close to the wall. We summarize the boundary integral formulation for the numerical implementation in § 2.1. We present the exact solution for a squirmer perpendicular to a flat no-slip wall in § 3. This exact solution allows us to derive an extended far-field formula, which we compare against the numerical results to validate the boundary integral code, and also examine the range of validity for the far-field approximation in § 3.1. We further study the near-field approximation to the flow and compare between the exact solution, boundary integral simulation results, and the asymptotic results in the literature in § 3.2. In § 4 we classify the swimming dynamics of a squirmer interacting with a no-slip planar wall under gravity, and show the detailed bifurcation structures for mixed squirming modes (§ 4.1) and pure squirming modes (§ 4.2). In § 5 we provide discussions of our results and implications for future directions.

2. Problem Formulation

We consider a three-dimensional incompressible viscous fluid governed by the equations of Stokes flow,

$$-\nabla p + \mu_f \nabla^2 \mathbf{u} = \mathbf{0}, \quad \nabla \cdot \mathbf{u} = 0, \quad (2.1)$$

for $\mathbf{x} \in \Omega$, the space between squirmers and a planar wall in Fig. (1). The squirmer is a sphere of radius R located at a height h above the planar wall, and has an orientation vector $\hat{\mathbf{e}}$ at an angle θ with respect to the wall: $\theta = 0$ when the squirmer is parallel to the wall, and $\theta = \pi/2$ when the squirmer is upright. Furthermore we assume that there is a density mismatch $\Delta\rho$ between

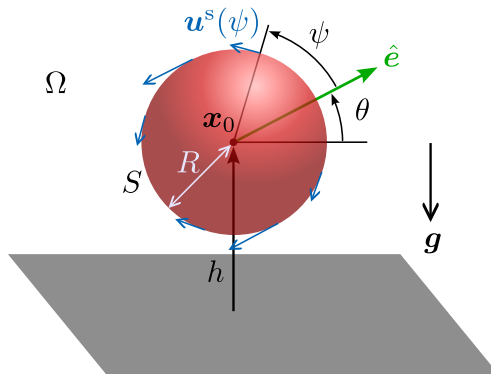


Figure 1: Schematic of a spherical squirmer of radius R at a height h above a no-slip planar boundary with gravity pointing toward the wall.

the viscous fluid and the squirmer, which sediments under gravity. For spherical squirmers of constant excess density $\Delta\rho$ relative to the surrounding fluid, the excess gravitational force on the squirmer is given by

$$\mathbf{F}^{\text{grav}} = -F^{\text{grav}} \hat{\mathbf{e}}_z = -\frac{4}{3}\pi R^3 g \Delta\rho \hat{\mathbf{e}}_z, \quad (2.2)$$

where g is the constant gravitational acceleration in the $-\hat{\mathbf{e}}_z$ direction, see Fig. (1).

We focus on fluid flow generated by the activity on the squirmer surface S , and assume that the fluid flow vanishes in the far-field. Furthermore we consider spherical squirmer with up to the first two squirming modes, prescribing either the tangential velocity or the tangential stress distribution. The prescribed surface tangential velocity distribution is purely in the polar ($\hat{\mathbf{e}}_\psi$) direction and is given by

$$\mathbf{u}^s = u_\psi \hat{\mathbf{e}}_\psi, \quad u_\psi = B_1 \sin(\psi) + B_2 \sin(\psi) \cos(\psi), \quad (2.3)$$

where ψ is the angle of the radial vector at a point on the surface to the orientation vector $\hat{\mathbf{e}}$ of the squirmer, see Fig. (1). B_1 is the neutral, self-propelling mode with swimming speed $V = 2B_1/3$ in free space ($V = 2/3$ when $B_1 = 1$). B_2 is the stresslet mode: $B_2 > (<)0$ for contractile puller (extensile pusher) squirmers. The velocity continuity and stress balance at the squirmer boundary and the planar wall provide the boundary conditions that close the system of equations.

In the simulations, we apply a repulsive force on the squirmer at a distance r (the bottom of the sphere to the wall) to the no-slip wall (Brady & Bossis 1985; Ishikawa *et al.* 2006)

$$F^{\text{rep}} = \frac{C^{\text{rep}} \exp(-a^{\text{rep}} r)}{1 - \exp(-a^{\text{rep}} r)}, \quad (2.4)$$

pointing away from the wall. We use numerical values $C^{\text{rep}} = 10^3$, $a^{\text{rep}} = 100$ to ensure a short-range repulsion, sufficient to maintain an equilibrium separation of $0.04R$ for a sphere of radius $R = 1$ and free space sedimentation speed $V_g = 1$ with no active squirming.

2.1. Numerical algorithm and validation

The incompressible velocity field \mathbf{u} that satisfies the Stokes equations (Eqs. (2.1)) can be expressed in terms of integrals of force and/or stress densities on the surfaces (Pozrikidis 1992). In particular, in the absence of a background flow, the i th component of the fluid velocity at a

point \mathbf{x} outside or on the surface S of a particle can be represented by a single-layer potential as

$$u_i(\mathbf{x}) = \int_S \mathbf{G}_{ij}(\mathbf{x}, \mathbf{y}) q_j(\mathbf{y}) dS(\mathbf{y}), \quad (2.5)$$

where \mathbf{G}_{ij} are the ij th components of the Green's function tensor \mathbf{G} for Stokes flow. In free space, the Green's function has the formula

$$\mathbf{G}_{ij}^{\text{FS}}(\mathbf{x}, \mathbf{y}) = \frac{\delta_{ij}}{r} + \frac{r_i r_j}{r^3}, \quad (2.6)$$

where $\mathbf{r} = \mathbf{x} - \mathbf{y}$ and $r = |\mathbf{r}|$. For simulations near a no-slip plane boundary, we use the modified Green's function $\mathbf{G} = \mathbf{G}^{\text{FS}} + \mathbf{G}^{\text{im}}$ so that the velocity field satisfies the no-slip boundary condition on the plane $z = 0$ by including image terms given by (Blake 1971a)

$$\mathbf{G}_{ij}^{\text{im}}(\mathbf{x}, \mathbf{y}) = -\frac{\delta_{ij}}{\tilde{r}} - \frac{\tilde{r}_i \tilde{r}_j}{\tilde{r}^3} + 2y_3 (\delta_{j\alpha} \delta_{\alpha l} - \delta_{j3} \delta_{3l}) \frac{\partial}{\partial \tilde{r}_l} \left[\frac{y_3 \tilde{r}_i}{\tilde{r}^3} - \left(\frac{\delta_{i3}}{\tilde{r}} + \frac{\tilde{r}_i \tilde{r}_3}{\tilde{r}^3} \right) \right], \quad (2.7)$$

where $\tilde{\mathbf{r}} = (x_1 - y_1, x_2 - y_2, x_3 + y_3)$, $\tilde{r} = |\tilde{\mathbf{r}}|$, and summations are implied over $\alpha = 1, 2$, and $l = 1, 2, 3$. In the case of a rigid body motion of the particle, the density \mathbf{q} of the single-layer potential is proportional to the traction vector \mathbf{f} ,

$$\mathbf{q} = -\frac{1}{8\pi\mu_f} \mathbf{f}. \quad (2.8)$$

For a squirmer with tangential surface velocity distribution \mathbf{u}^s moving with translational velocity \mathbf{U} and rotational velocity $\boldsymbol{\Omega}$ about its center \mathbf{x}_0 , we have the boundary condition

$$\mathbf{U} + \boldsymbol{\Omega} \times (\mathbf{x} - \mathbf{x}_0) + \mathbf{u}^s = \int_S \mathbf{G}(\mathbf{x}, \mathbf{y}) \mathbf{q}(\mathbf{y}) dS(\mathbf{y}) \quad (2.9)$$

for $\mathbf{x} \in S$.

The total hydrodynamic force acting on the particle or droplet is given by

$$\mathbf{F}^{\text{hydro}} = -8\pi\mu_f \int_S \mathbf{q}(\mathbf{y}) dS(\mathbf{y}) \quad (2.10)$$

and the total hydrodynamic torque is

$$\mathbf{L}^{\text{hydro}} = -8\pi\mu_f \int_S \mathbf{y} \times \mathbf{q}(\mathbf{y}) dS(\mathbf{y}). \quad (2.11)$$

For squirmers that experience forces due to gravity and short-range repulsion, we impose the force balance equation

$$\mathbf{F}^{\text{hydro}} + \mathbf{F}^{\text{rep}} + \mathbf{F}^{\text{grav}} = \mathbf{0}. \quad (2.12)$$

By symmetry, gravity and short-range repulsion do not exert torques on the spherical squirmers so the torque balance equation is

$$\mathbf{L}^{\text{hydro}} = \mathbf{0}. \quad (2.13)$$

The full system of equations to be solved at a given time consists of (2.9), (2.12), and (2.13). To solve this system numerically, the surface of the squirmer is discretized into quadratic triangular elements and the density \mathbf{q} is approximated by a quadratic interpolation of the values at the six nodes of each triangular element. In this work we prescribe the tangential velocities \mathbf{u}^s in (2.9) at each of the N nodes on the surface of the squirmer, and the single-layer density \mathbf{q} at the nodes are unknowns, as are the translational and rotational velocity vectors. This yields $3N$ equations in $(3N + 6)$ unknowns. Six further equations arise from the force and torque balance constraints.

3. Exact solutions for a squirmer perpendicular to a planar wall under gravity

We next assume that the squirmer orientation vector \hat{e} is normal to the planar wall, pointing towards the wall ($\theta = -\pi/2$). Under such axial symmetry, we compute the axisymmetric flow generated by the squirmer interacting with a planar wall using bipolar spherical coordinates defined as

$$z + i\varrho = ic \cot \frac{1}{2} (\eta + i\xi), \quad (3.1)$$

where ϱ and z are the cylindrical coordinates that can be expressed explicitly in terms of η and ξ :

$$\varrho = \frac{c \sin \eta}{\cosh \xi - \cos \eta}, \quad x = \frac{c \sinh \xi}{\cosh \xi - \cos \eta}, \quad (3.2)$$

with $2c$ the distance between the two poles of the bispherical coordinates. In the present application it is only necessary to consider the situation $\varrho > 0$ which corresponds to $0 \leq \xi < \infty$ and $0 \leq \eta \leq \pi$. $\xi = 0$ corresponds to a plane, $\xi = \zeta = \text{arcosh}(h/R)$ corresponds to a spherical surface of radius $c/\sinh \zeta$ centered at $c \coth \xi$. In axisymmetric flow, one can write the velocity as a curl of a vector, $\mathbf{u} = \nabla \times (\varphi(\xi, \eta) \hat{e}_\phi)$, with \hat{e}_ϕ being the unit vector in the azimuthal direction and $\varphi(\xi, \eta)$ being the Stokes stream function. Accordingly, the governing differential equation for the axisymmetric viscous flow reduces to a fourth order linear differential equation for φ :

$$D^4 \varphi = (D^2)^2 \varphi = 0, \quad (3.3)$$

where the differential operator D^2 in bispherical coordinates is given by

$$D^2 \equiv \frac{\cosh \xi - \mu}{c^2} \left\{ \frac{\partial}{\partial \xi} \left[(\cosh \xi - \mu) \frac{\partial}{\partial \xi} \right] + (1 - \mu^2) \frac{\partial}{\partial \mu} \left[(\cosh \xi - \mu) \frac{\partial}{\partial \mu} \right] \right\} \quad (3.4)$$

with $\mu(\eta) = \cos \eta$. The general expression for the stream function φ can be given in the bispherical coordinates (Stimson & Jeffery 1926)

$$\varphi(\xi, \eta) = (\cosh \xi - \cos \eta)^{-3/2} \sum_{n=1}^{\infty} \chi_n(\xi) V_n(\mu(\eta)), \quad (3.5)$$

$$\chi_n(\xi) = A_n \cosh \left(n - \frac{1}{2} \right) \xi + B_n \sinh \left(n - \frac{1}{2} \right) \xi + C_n \cosh \left(n + \frac{3}{2} \right) \xi + D_n \sinh \left(n + \frac{3}{2} \right) \xi, \quad (3.6)$$

$$V_n(\mu(\eta)) = P_{n-1}(\cos \eta) - P_{n+1}(\cos \eta), \quad (3.7)$$

where P_n is the n th order Legendre polynomial. We can express the components of velocity in terms of the stream function as

$$u_\xi = \frac{(\cosh \xi - \cos \eta)^2}{c \sin \eta} \frac{\partial \varphi}{\partial \eta} \quad (3.8)$$

$$= -\frac{3}{2c\sqrt{\cosh \xi - \cos \eta}} \sum_{n=1}^{\infty} \chi_n(\xi) V_n(\mu) + \frac{\sqrt{\cosh \xi - \cos \mu}}{c \sin \eta} \sum_{n=1}^{\infty} \chi_n(\xi) \frac{\partial V_n(\mu)}{\partial \eta},$$

$$u_\eta = -\frac{(\cosh \xi - \cos \eta)^2}{c \sin \eta} \frac{\partial \varphi}{\partial \xi} \quad (3.9)$$

$$= \frac{3 \sinh \xi}{2c \sin \eta \sqrt{\cosh \xi - \cos \eta}} \sum_{n=1}^{\infty} \chi_n(\xi) V_n(\mu) - \frac{\sqrt{\cosh \xi - \cos \mu}}{c \sin \eta} \sum_{n=1}^{\infty} \chi'_n(\xi) V_n(\mu).$$

For each (n th) term of the stream function expansion φ there are four coefficients A_n, B_n, C_n and D_n to be determined as a function of the squirmer speed U according to the boundary conditions

of the rigid body motion and velocity continuity on the squirmer surface and the planar wall. Assuming axisymmetry (see Fig. (1)), we use the force-free condition to compute the squirmer velocity U in the downward vertical direction as

$$U = 2 \frac{\mathcal{B}_1(\zeta)}{\lambda_B(\zeta)} B_1 - \frac{8}{3} \frac{\mathcal{B}_2(\zeta)}{\lambda_B(\zeta)} B_2 + \frac{F^{\text{grav}} - F^{\text{rep}}}{8\pi\mu_f R \lambda_B(\zeta)}, \quad (3.10)$$

$$\lambda_B(\zeta) = \sinh \zeta \sum_{n=1}^{\infty} \frac{n(n+1)}{(2n-1)(2n+3)\Delta_n} [2 \sinh(2n+1)\zeta + (2n+1) \sinh 2\zeta - \Delta_n], \quad (3.11)$$

$$\mathcal{B}_1(\zeta) = \sinh^3 \zeta \sum_{n=1}^{\infty} \frac{n(n+1)}{\Delta_n} [1 - \cosh(2n+1)\zeta + \sinh(2n+1)\zeta], \quad (3.12)$$

$$\mathcal{B}_2(\zeta) = \sinh^2 \zeta \sum_{n=1}^{\infty} \frac{n(n+1)}{(2n-1)(2n+3)} \sinh \left(\left(n + \frac{1}{2} \right) \zeta \right) \frac{M_2(n, \zeta)}{\Delta_n}, \quad (3.13)$$

$$M_2(n, \zeta) = \sinh \zeta (n-1)(n+2) \left[(2n+3)e^{-(n-\frac{1}{2})\zeta} - (2n-1)e^{-(n+\frac{3}{2})\zeta} \right] - \quad (3.14)$$

$$\frac{5}{4} \left[(n-1)(2n+3)e^{-(n-\frac{3}{2})\zeta} + (2n+1)e^{-(n+\frac{1}{2})\zeta} - (n+2)(2n-1)e^{-(n+\frac{5}{2})\zeta} \right],$$

$$\Delta_n = 4 \sinh^2 \left(n + \frac{1}{2} \right) \zeta - (2n+1)^2 \sinh^2 \zeta. \quad (3.15)$$

The drag coefficient for vertical motion in the presence of the no-slip wall is $c_D(\zeta) = 8\pi\mu_f \lambda(\zeta)$ and the individual contributions to the net velocity from B_1 , B_2 , gravity, and repulsion are identified as

$$U_1 = 2 \frac{\mathcal{B}_1(\zeta)}{\lambda_B(\zeta)} B_1, \quad (3.16)$$

$$U_2 = -\frac{8}{3} \frac{\mathcal{B}_2(\zeta)}{\lambda_B(\zeta)} B_2, \quad (3.17)$$

$$U^{\text{grav}} = \frac{F^{\text{grav}}}{8\pi\mu_f R \lambda_B(\zeta)} = V_g \cdot \frac{3}{4\lambda_B(\zeta)}, \quad (3.18)$$

$$U^{\text{rep}} = -\frac{F^{\text{rep}}}{8\pi\mu_f R \lambda_B(\zeta)}, \quad (3.19)$$

respectively, where $V_g = 2g\Delta\rho R^2/9\mu_f$ is the terminal velocity of the passive sphere in free space. We remark that in the situation where the squirmer is pointing vertically upwards ($\theta = +\pi/2$), the velocities (still expressed in the downward direction) are unchanged from the corresponding formulas in (3.16)–(3.19) apart from a change in sign in (3.16).

3.1. Far-field expansion of U for a squirmer near a wall

The expression for the squirmer speed in Eq. (3.10) allows for a far-field expansion of U in the limit of $\zeta \rightarrow \infty$. In the absence of squirming activity ($B_1 = B_2 = 0$), the speed of a squirmer under gravity is

$$U^{\text{grav}} = V_g \left(1 - \frac{9R}{8h} + \frac{1}{2} \left(\frac{R}{h} \right)^3 - \frac{135}{256} \left(\frac{R}{h} \right)^4 - \frac{1}{8} \left(\frac{R}{h} \right)^5 + \frac{401}{512} \left(\frac{R}{h} \right)^6 - \frac{675}{1024} \left(\frac{R}{h} \right)^7 \cdots \right). \quad (3.20)$$

Eq. (3.20) is identical, up to $O((R/h)^3)$, to the often-used expression derived from the method of images with one image. The activity on the squirmer surface (B_1 and B_2) contributes to the

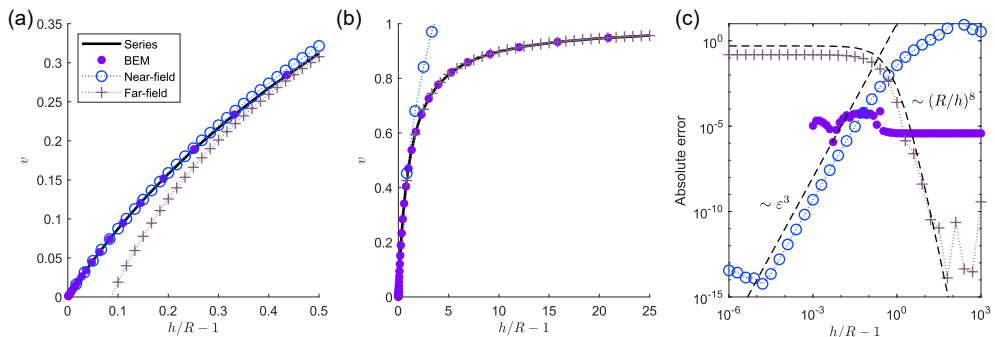


Figure 2: Comparison of the series expression (3.10) with series truncated to 5000 terms, boundary integral simulation solutions, the near-field formula (3.22), and the far-field formula (3.20) for the vertical speed $v = U^{\text{grav}}/V_g$ of a passive sphere ($B_1 = B_2 = 0$) sedimenting under gravity near a no-slip wall without repulsion. Parts (a) and (b) display the same quantities focusing over different ranges of separation from the wall. (c) Errors with respect to the series solution.

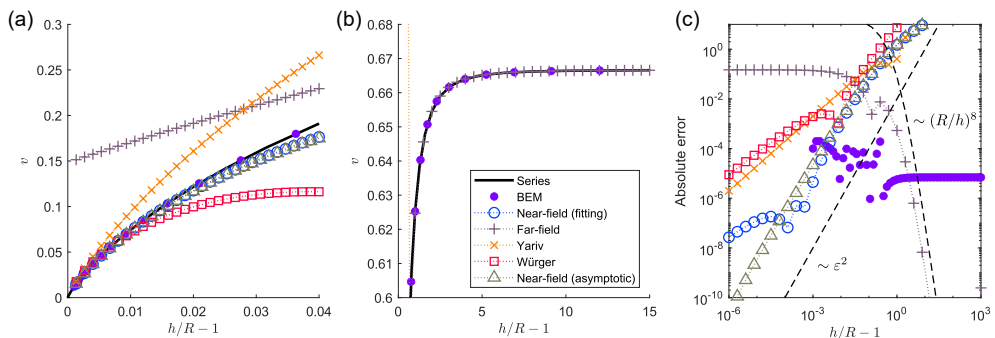


Figure 3: Comparison of the series expression (3.10) with series truncated to 5000 terms, boundary integral simulation solutions, the near-field formula (3.27), and the far-field formula (3.21) for the vertical speed of a neutral squirmer ($B_1 = 1, B_2 = 0, V_g = 0$) perpendicular to and near a no-slip wall without repulsion. Parts (a) and (b) display the same quantities focusing over different ranges of separation from the wall. (c) Errors with respect to the series solution.

far-field squirmer speed as

$$\begin{aligned}
 U = U^{\text{grav}} + B_1 \left(\frac{2}{3} - \frac{1}{3} \left(\frac{R}{h} \right)^3 + \frac{1}{6} \left(\frac{R}{h} \right)^5 - \frac{45}{128} \left(\frac{R}{h} \right)^6 + \dots \right) + \\
 B_2 \left(\frac{3}{8} \left(\frac{R}{h} \right)^2 - \frac{1}{2} \left(\frac{R}{h} \right)^4 + \frac{15}{32} \left(\frac{R}{h} \right)^5 + \frac{5}{24} \left(\frac{R}{h} \right)^6 - \frac{441}{512} \left(\frac{R}{h} \right)^7 + \dots \right).
 \end{aligned} \tag{3.21}$$

3.2. Near-field U for a squirmer near a wall

Cox & Brenner (1967) and Cooley & O'Neill (1969) provided an expression for the near-field velocity of a sedimenting rigid sphere ($B_1 = B_2 = 0$) at a distance h above a planar wall, with

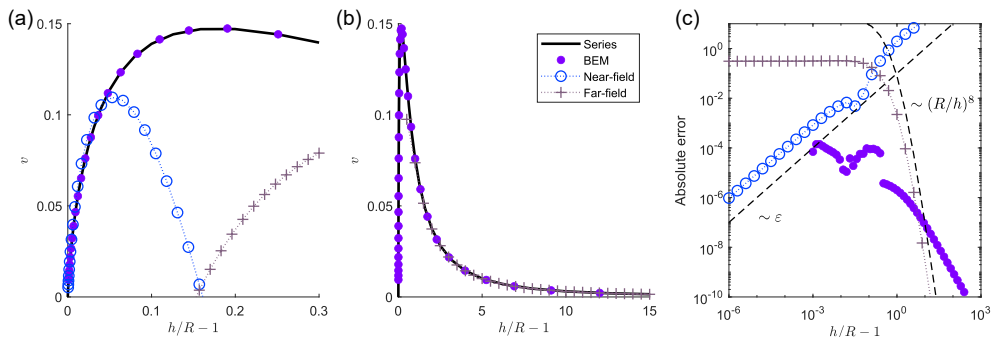


Figure 4: Comparison of the series expression (3.10) with series truncated to 5000 terms, boundary integral simulation solutions, the near-field formula (3.27), and the far-field formula (3.21) for the vertical speed of a contractile squirmer ($B_1 = 0$, $B_2 = 1$, $V_g = 0$) perpendicular to and near a no-slip wall without repulsion. Parts (a) and (b) display the same quantities focusing over different ranges of separation from the wall. (c) Errors with respect to the series solution.

$\varepsilon = h/R - 1 \ll 1$ and $\zeta = \text{arcosh}(1 + \varepsilon)$,

$$U^{\text{grav}} = \frac{\frac{4}{3}\pi R^3 \Delta\rho g}{6\pi\mu_f R} \frac{1}{\varepsilon^{-1} - (0.2 \ln \varepsilon - 0.971280)} \quad (3.22)$$

$$= V_g \frac{1}{\varepsilon^{-1} - (0.2 \ln \varepsilon - 0.971280)}. \quad (3.23)$$

This result shows that the infinite series λ_B in the denominators on the right-hand-side of Eq.(3.10) has the following asymptotic behavior as $\varepsilon \rightarrow 0$:

$$\lambda_B(\zeta(\varepsilon)) \rightarrow \overline{\lambda_B} \equiv \frac{3}{4} \left(\varepsilon^{-1} - 0.2 \ln \varepsilon + 0.971280 \right). \quad (3.24)$$

This is confirmed in Fig. (2), showing both the truncated series solution and the boundary integral simulation results are in good agreement with the near-field asymptotic expression in Eq. (3.22).

For a squirmer with a prescribed slip velocity $B_1 \neq 0$ and $B_2 = 0$ moving towards the wall ($\theta = -\pi/2$), Yariv (2016) provided an asymptotic expression for the near-field velocity (adapted to our variable definitions)

$$U_1 \approx -2B_1\varepsilon (\ln \varepsilon - 0.1087), \quad (3.25)$$

which corresponds to

$$\mathcal{B}_1(\zeta(\varepsilon)) \approx -\frac{3}{4}(\ln \varepsilon - 0.1087). \quad (3.26)$$

Würger (2016) considered a simplifying assumption and derived an asymptotic result where the constant -0.1087 in (3.25) is replaced by $+2.25$. Based on the results in Eqs. (3.24)-(3.26), we construct an ansatz for the near-field behavior of the squirmer speed in Eq. (3.10), assuming identical forms for the approximations to \mathcal{B}_1 and \mathcal{B}_2 , with $\varepsilon \ll 1$:

$$U \approx \frac{1}{\lambda_B} \left[2B_1 a_1 (\ln \varepsilon + b_1) - \frac{8}{3} B_2 a_2 (\ln \varepsilon + b_2) + \frac{3}{4} V_g \right], \quad (3.27)$$

We then compute the coefficients a_1 , b_1 , a_2 , and b_2 by least-squares fitting of the series solution truncated at 5000 terms over the range $10^{-5} \leq \varepsilon \leq 10^{-3}$ to Eq. (3.27), and obtain:

$$a_1 = -0.7476, \quad b_1 = 0.8633, \quad a_2 = 1.006, \quad b_2 = 1.825. \quad (3.28)$$

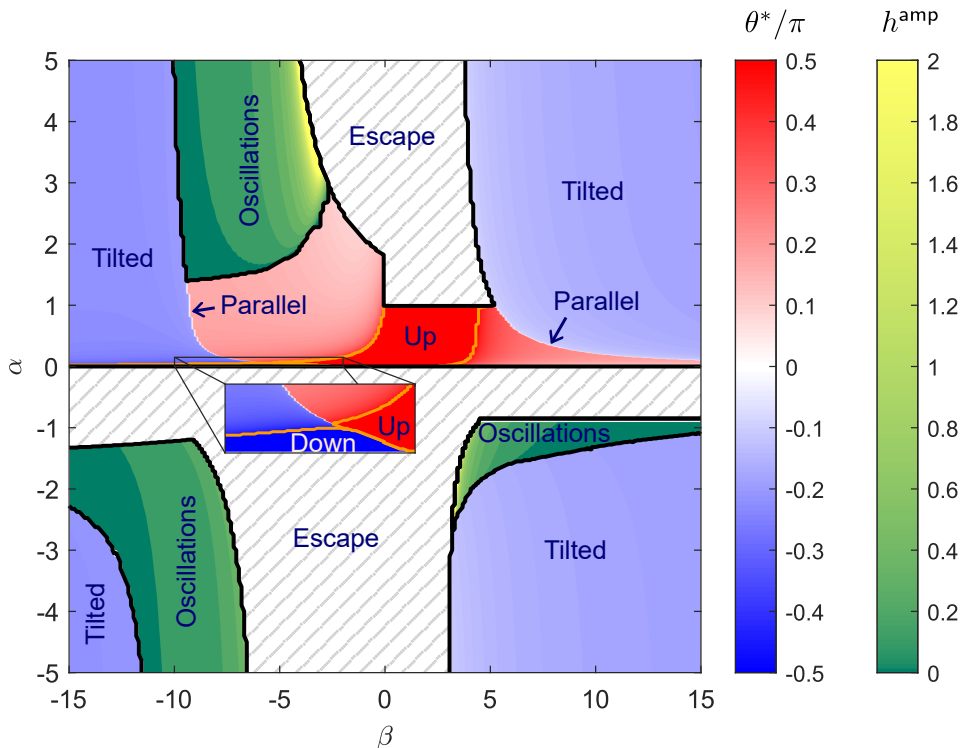


Figure 5: Long-time behaviors of a squirmer under gravity next to a flat wall, with the squirmer initially pointing nearly vertically downwards ($\theta(t=0) = -0.99\pi/2$) at a starting height $h/R = 10$. The squirmer is not bound to the wall in the “Escape” region. For squirmers bound to the wall under gravity, they settle to either a steady state at a fixed height with a steady tilt angle sliding along the wall (red–blue color bar), or they oscillate in the “Oscillations” region where the squirmer–wall distance oscillates with amplitudes in height indicated by the right (green–yellow) color bar. Negative values of α signify that gravity acts vertically away from the wall. The inset shows the detailed distribution of swimming dynamics for $0 < \alpha < 0.15$ and $-10 < \beta < -2$.

As an independent check, we apply the methods in Cox & Brenner (1967) to compute the near-field asymptotic expansion for a squirmer with $B_1 = 1$ and $B_2 = 0$, and find $a_1 = -0.75$ and $b_1 = 0.8913$, in good agreement with the values from the least-squares fitting.

We next compare the asymptotic near-field results from both (Yariv 2016) and (Würger 2016) with our boundary integral simulation results and our near-field expression in Eq. (3.27) in Fig. (3) with $B_1 = 1$ and $B_2 = 0$. We find that our near-field expression in Eq. (3.27)–(3.28) is close to the truncated series solution for $10^{-6} \leq \varepsilon \leq 0.05$ and close to the boundary integral simulation for $10^{-3} \leq \varepsilon \leq 0.05$ (the boundary integral solution is not accurate for $\varepsilon < 10^{-3}$), while the asymptotic expressions from both Yariv (2016) and Würger (2016) diverge significantly for $\varepsilon \geq 0.02$. For $B_1 = 0$ and $B_2 = 1$ we compare our near-field expression with the truncated series and boundary integral simulation results in Fig. (4).

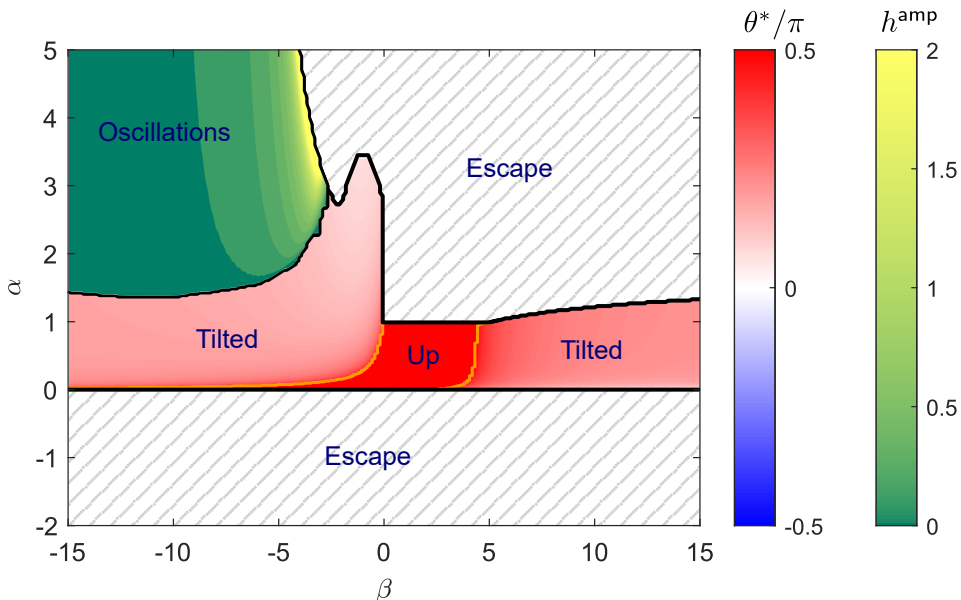


Figure 6: Long-time behaviors of a squirmer under gravity next to a flat wall, with the squirmer initially pointing horizontally (parallel to the wall) at a starting height $h/R = 10$. The squirmer is not bound to the wall in the “Escape” region. For squirmers bound to the wall under gravity, they settle to either a steady state at a fixed height with a steady tilt angle (red–blue color bar), or they oscillate in the “Oscillations” region where the squirmer-wall distance oscillates with amplitudes in height indicated by the right (green–yellow) color bar. Negative values of α signify that gravity acts vertically away from the wall.

4. Swimming dynamics of a squirmer under gravity near a no-slip wall

4.1. Classification of squirmer dynamics in the $\alpha - \beta$ plane

Under gravity, various types of swimming dynamics arise from the hydrodynamic interaction between a squirmer and a no-slip flat wall (Li & Ardekani 2014; Lintuvuori *et al.* 2016; Rühle *et al.* 2018; Théry *et al.* 2023). We first define two parameters to quantify such diverse swimming dynamics: (i) $\alpha = V/V_g$, the ratio of self-propulsion speed due to B_1 mode to the gravity-induced speed, and (ii) $\beta = B_2/B_1$, the ratio of the two squirmering mode magnitudes.

For $\alpha > 1$, the squirmer is prone to escape from the wall in the long-time limit, even though its initial height and orientation may lead to a transient contact with the wall. We consider a trajectory to have escaped the wall if $h/R > 100$ at any positive time. For a squirmer that is bound to the wall, at least three types of swimming dynamics have been reported: (1) The squirmer is pinned close to the wall at a fixed height, pointing either toward or away from the wall, depending on the values of (α, β) . (2) The squirmer slides along the wall at a fixed height with a tilted orientation. (3) The squirmer oscillates (bounces) in both height and orientation. While these near-wall swimming dynamics under gravity have been reported in the literature (Li & Ardekani 2014; Rühle *et al.* 2018), no detailed investigation on how these states may bifurcate in terms of (α, β) is available to our knowledge.

From both numerical simulations and far-field analysis, we find that the squirmer is less likely to be bound to the wall if its initial orientation points away from the wall. Thus we first focus on the various dynamics of a squirmer initially pointing towards the flat wall. We use the efficient and accurate boundary integral codes to evaluate the velocities of the squirmer on a grid in (θ, h)

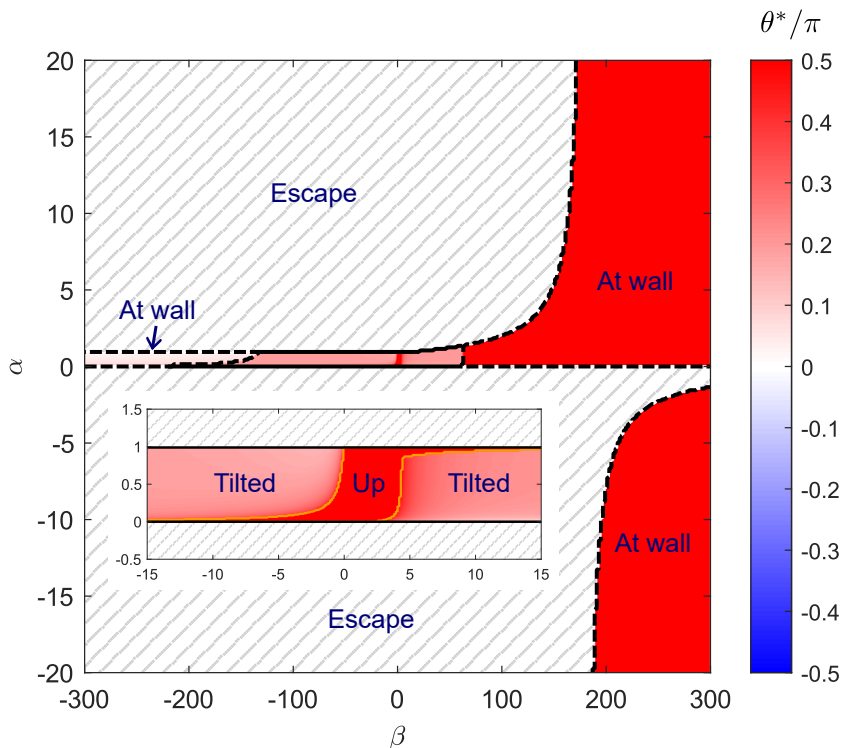


Figure 7: Long-time behaviors of a squirmer under gravity next to a flat wall, with the squirmer initially pointing nearly vertically upwards ($\theta(t=0) = 0.99\pi/2$) at a starting height $h/R = 10$. The squirmer is not bound to the wall in the “Escape” region. For squirmers bound to the wall under gravity, they settle to either a steady state at a fixed height with a steady tilt angle indicated by the color bar. In regions labelled as “at wall,” the squirmer approaches the minimum wall separation for which velocities were computed so trajectories could not be continued further in time. Negative values of α signify that gravity acts vertically away from the wall. An inset shows more detail for the range $-0.5 < \alpha < 1.5$, $-15 < \beta < 15$.

configuration space. We then compute streamlines to map out the various squirming dynamics in the (α, β) -plane for a squirmer initially pointing nearly vertically down (specifically, the initial orientation angle is $\theta_0 = -0.99\pi/2$) at a height of $h_0 = 10R$. The various swimming dynamics is summarized in Fig. (5). For pinned and sliding dynamics we color code their regions using the orientation angle, with $\theta^* = \pi/2$ pointing up (red) and $\theta^* = -\pi/2$ pointing down (blue). The region for oscillatory dynamics is color coded by the oscillation amplitude (h^{amp}) of squirmer height (green). We note that while oscillations can be obtained over a large region of parameter space, the amplitudes are small except near the boundary with escaping behavior. Fig. (6) shows the distribution of swimming dynamics for a squirmer initially parallel to the wall. For a squirmer initially pointing away from the wall (vertically up), Fig. (7) shows that the squirmer can stay bound to the wall for a wider range of α for $\beta \gg 1$, when the upward pointing squirmer moves toward the wall and stays bound to the wall for $|\alpha| \gg 1$ due to the strong puller mode $B_2 \gg B_1$.

The squirmer dynamics summarized in Figs. (5-7) offer some general observations: (1) A squirmer stays bound to the bottom wall under gravity as long as α is in the range $\alpha \in [0, 1]$ for all values of β . (2) The oscillatory dynamics of a squirmer under gravity is generally associated with negative β (extensile squirmers). When gravity is directed away from the wall (for example,

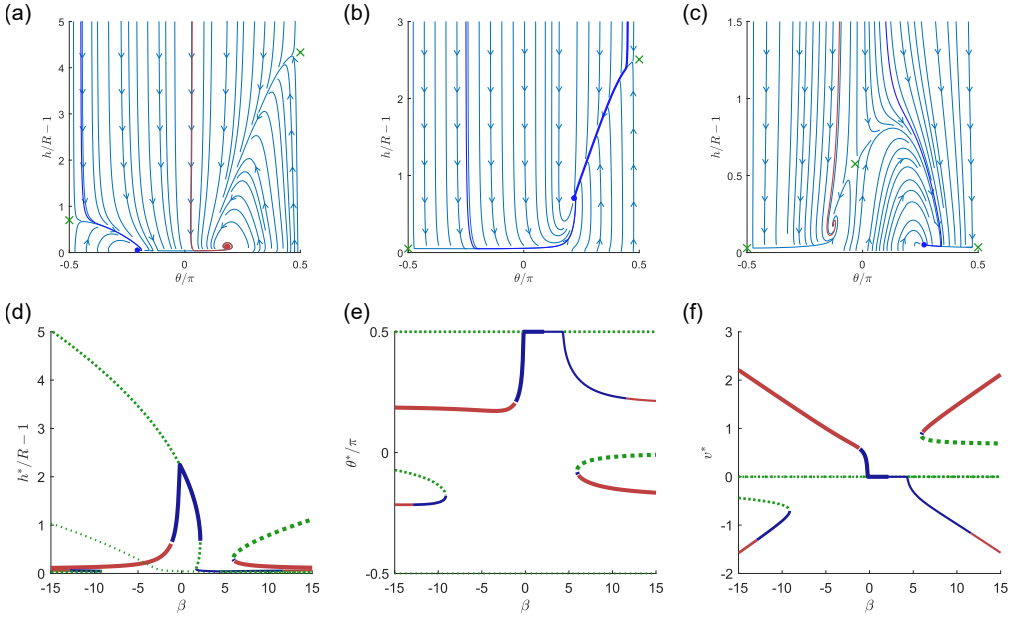


Figure 8: Bifurcation structures of swimming dynamics of a squirmer with $\alpha = 2/3$. Top row: (a) $\beta = -10$, with two saddles (crosses), a stable node (blue filled circle), and a stable spiral, (b) $\beta = -1$, with two saddles and a stable node, and (c) $\beta = 7.5$, with three saddles, a stable node, and a stable spiral. Bottom row: Dependence of (d) stable height, (e) orientation, and (f) wall-parallel speed on β . Red curves indicate stable spirals and blue curves indicate stable nodes. Green dashed curves indicates saddle nodes. Different curve thicknesses are used to visually distinguish branches of stationary points.

if the wall is at the top of a chamber), however, it is possible to observe oscillatory dynamics for both contractile and extensile squirmers. (3) For a squirmer initially pointed towards the wall the squirmer can be pinned facing down, albeit in a very small region (insert of Fig. (5)). (4) The squirmer does not bounce (oscillate) around the wall if it initially points away from the wall. (5) For sufficiently large β we expect that a squirmer can be bound to the wall, independent of squirmer's initial configuration and the value of $\alpha > 0$.

We next examine the detailed bifurcation structures of squirmer swimming dynamics as a function of β for various fixed values of α . An example is shown in Fig. (8), where $\alpha = 2/3$ and we vary $\beta = B_2/B_1$ with $B_1 = 1$ and $C^{\text{rep}} = 10^4$. We quantify the swimming dynamics via the equilibrium states (the fixed points) in the flow map of the squirmer in the plane of height versus angle. In the top row of Fig. (8), the red curves are for stable spirals and blue curves are for stable nodes in the flow map. A stable spiral and a stable node are found for $\beta = -10$ in (a) and $\beta = 7.5$ in (c). In (b), only one stable node is found for $\beta = -1$. The bottom row summarizes the bifurcation structures for $\beta = B_2/B_1 \in [-15, 15]$, with the dotted curves denoting the unstable branches.

At a higher squirmer propulsion speed (higher value of α), we expect the region for stable nodes to shrink. An example with $\alpha = 5$ is shown in Fig. (9). In the top row, the phase plane diagrams are shown for $\beta = -12$ in (a), -2 in (b), and 5 in (c). For $\beta = -12$, squirmers that approach the wall are attracted either to a stable node with a negative tilt or to a limit cycle with positive tilt; both of these attractors are very close to the wall. For $\beta = -2$, most initial conditions lead to escape from the wall but some are attracted to a stable spiral. For $\beta = 5$ (c), the squirmer

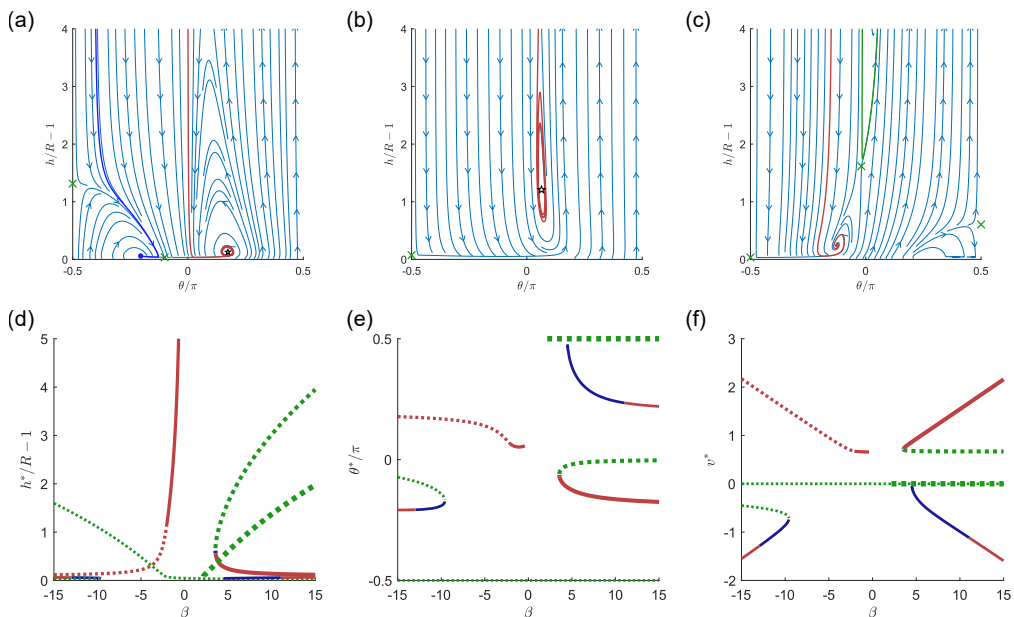


Figure 9: Bifurcation structures of swimming dynamics of a squirmer with $\alpha = 5$. Top row: (a) $\beta = -12$, with two saddles (crosses), a stable node (filled circle), and an unstable spiral (star) enclosed by a limit cycle, (b) $\beta = -2$, with a saddle and a stable spiral (for clarity, only a portion of a trajectory attracted to the spiral is shown), and (c) $\beta = 5$, with three saddles and a stable spiral. Bottom row: Dependence of (d) stable height, (e) orientation, and (f) wall-parallel speed on β . Red curves indicate stable spirals and blue curves indicate stable nodes. Green dashed curves indicates saddle nodes. Different curve thicknesses are used to visually distinguish branches of stationary points.

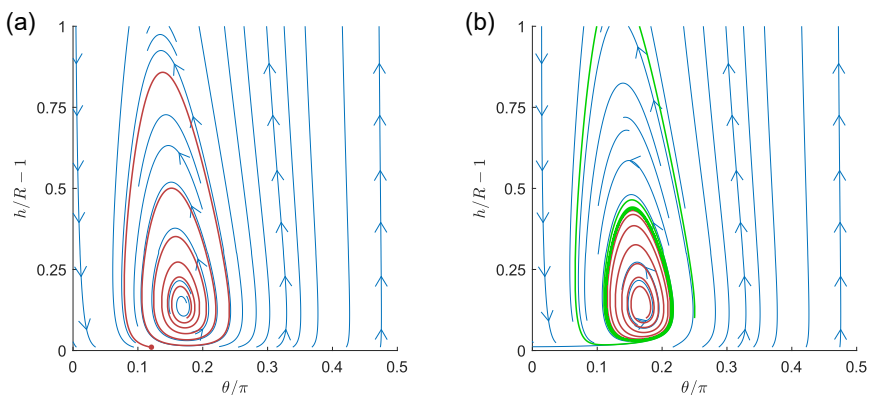


Figure 10: Effect of repulsion on the swimming dynamics of a squirmer with $\beta = -10$ ($B_1 = 1$, $B_2 = -10$), and $\alpha = 5$. Phase plane dynamics near an unstable spiral point (a) with no wall repulsion, and (b) with short-range wall repulsion given in Eq. 2.4. Red curves show trajectories starting close to the spiral point. The red dot in (a) (with no repulsion) indicates where the trajectory terminates due to close proximity with the wall. With repulsion in (b), the trajectory approaches a limit cycle, in which the distance from the wall and the orientation of the squirmer oscillate periodically. A trajectory starting outside this limit cycle is also shown (green).

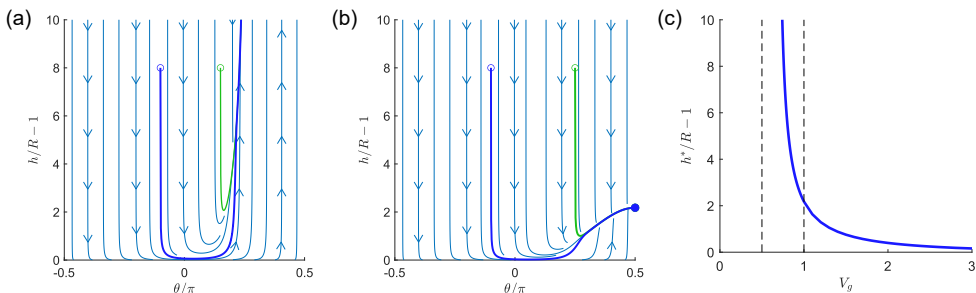


Figure 11: Threshold in V_g for a steady equilibrium height and angle for a squirmer with $B_1 = 1$, $B_2 = 0$ (neutral swimmer). (a) Escaping dynamics for a squirmer with $V_g = 0.5$. (b) A squirmer with $V_g = 1$ reaches a steady equilibrium height and points upward. (c) Dependence of stable height in perpendicular-up orientation on the free space sedimentation speed V_g . Dashed vertical lines indicate the values of V_g used in (a) and (b) respectively.

either spirals into a fixed point close to the wall or escapes, depending on the initial angle. There is an additional stable node close to the wall that cannot be reached by trajectories that begin far from the wall. The bifurcations with respect to β are summarized in the bottom row of Fig. (9). We find that the branch of stable nodes that was present for $\alpha = 2/3$ (blue curves in Fig. (8)) at intermediate values of β disappear at $\alpha = 5$. In fact, we find no stable equilibrium points for $\beta \in (-9.5, -2.07) \cup (0, 3.5)$. For $\beta < -2.07$, there is an unstable spiral around which we expect a limit cycle (as shown in Fig. (9a)) and for $\beta \in (0, 3.5)$, the generic behavior is to escape from the wall.

Fig. (10) shows the effect of wall repulsion on the spiraling squirmer dynamics, which transitions from (a) an unstable spiral that eventually becomes too close to the wall for numerical solutions to continue into (b) a limit cycle, giving rise to oscillatory dynamics of a squirmer in both height and orientation due to a wall repulsion that is strong enough to maintain a minimum separation between the wall and the squirmer.

4.2. Effects of gravity (varying V_g) for a pure squirmer

Here we investigate the swimming dynamics of a pure squirmer (either a “shaker” with $B_1 = 0$, $B_2 \neq 0$ or a “neutral swimmer” with $B_1 \neq 0$, $B_2 = 0$) under gravity, focusing on three combinations of (B_1, B_2) : $(1, 0)$ for a neutral swimmer in Fig. (11), $(0, 1)$ for a contractile shaker (puller) in Fig. (12) and $(0, -1)$ for an extensile shaker (pusher) in Fig. (13), and examine the swimming dynamics as a function of V_g .

For a neutral swimmer with $B_1 = 1$ and $B_2 = 0$, we find that it can be bound to the wall and stay at an equilibrium height, pointing toward the wall with zero velocity ($v^* = 0$) as long as the gravity is sufficiently large so that $V_g > 2/3$, see Fig. (11).

Slightly more complicated swimming dynamics is found for a contractile puller shaker ($B_1 = 0$ and $B_2 = 1$): We find a branch of saddle nodes where the squirmer points to the wall with zero velocity at a finite height. Co-existent with this saddle node is a stable spiral with a tilt angle and a sliding velocity for intermediate gravity. For sufficiently large V_g , the purely extensile squirmer is bound to the wall at a fixed height, pointing to the wall with zero velocity. Furthermore we find that for a contractile puller shaker under a sufficiently large V_g , the squirmer can reach an equilibrium height with its director parallel to the wall and a zero sliding velocity, see Fig. (12)(e) and (f), where the angle $\theta^* = 0$ and $v^* = 0$ for $V_g \geq 1$.

The bifurcation structure of the swimming dynamics of an extensile pusher shaker is summarized in Fig. (13), where we find that the steady state ($v^* = 0$ for large V_g) is a squirmer at a steady

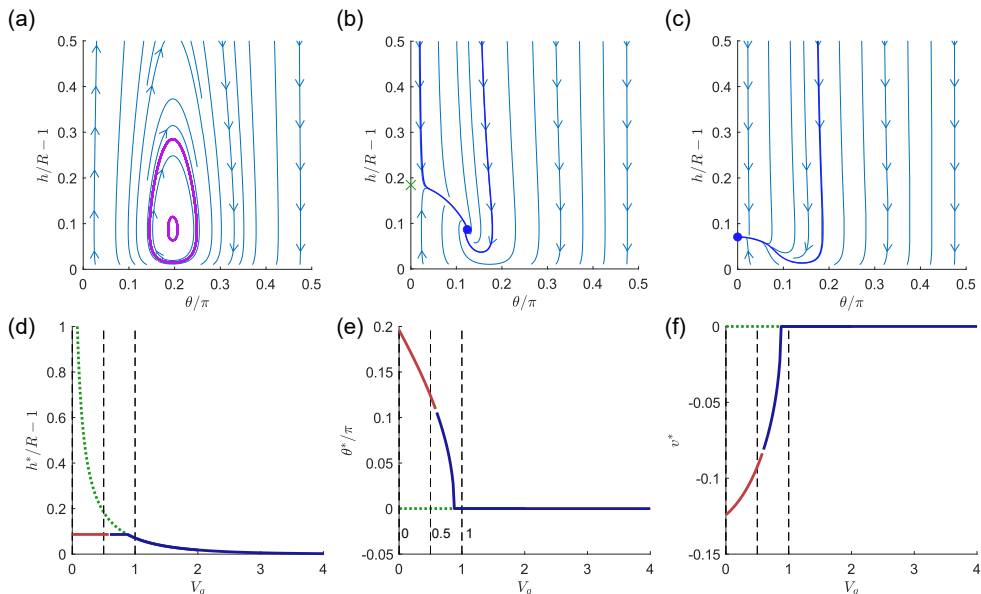


Figure 12: Bifurcation structures of swimming dynamics of a squirmer with $B_1 = 0, B_2 = 1$ (contractile shaker). Top row (a) $V_g = 0$, (b) $V_g = 0.5$, and (c) $V_g = 1$. Bottom row: Dependence of (a) stable height, (b) orientation, and (c) wall-parallel speed on the free space sedimentation speed V_g . Red curves indicate stable spirals and blue curves indicate stable nodes. Green dashed curves indicates saddle nodes.

equilibrium height while pointing upright, see Fig. (13)(e) and (f), where the angle $\theta^* = \pi/2$ and $v^* = 0$ for $V_g \gtrsim 1.6$.

5. Discussion and Conclusion

In this work we provide an exact solution for a spherical squirmer sedimenting to a flat solid wall. We provide both far-field and near-field approximations to the swimming velocity of a squirmer under gravity, and show that our near-field approximations, different from both (Yariv 2016) and (Würger 2016), are valid over a wider range of squirmer distances to the wall. We next use boundary integral simulations to map out its various swimming dynamics in the $\alpha - \beta$ plane, and find that the squirmer may escape from the wall, slide along the wall at a fixed height and orientation, stay at a fixed height pointing to or away from the wall, or oscillate in both height and orientation.

We further examine the bifurcations in the steady state configurations of the squirmer interacting with a solid wall as the parameters α and β are varied, identifying branches of stable and unstable spirals, stable nodes, and saddle nodes in $\theta-h$ phase space. In particular, we find that there are parameter regions where different swimming dynamics coexist (overlying solid branches for stable spiral and stable node in Figs. (8-9)). Such identification allows us to characterize when the squirmer will escape from the wall, remain bound to the wall at a fixed location, slide along the wall at a fixed height, or bounce along the wall, making it possible to design robotic microswimmers that can adjust their gaits (by changing the values of B_1 and B_2) to navigate along the solid wall in the presence of obstacles.

Particle-wall interactions in complex biological fluids often involve effects of non-Newtonian

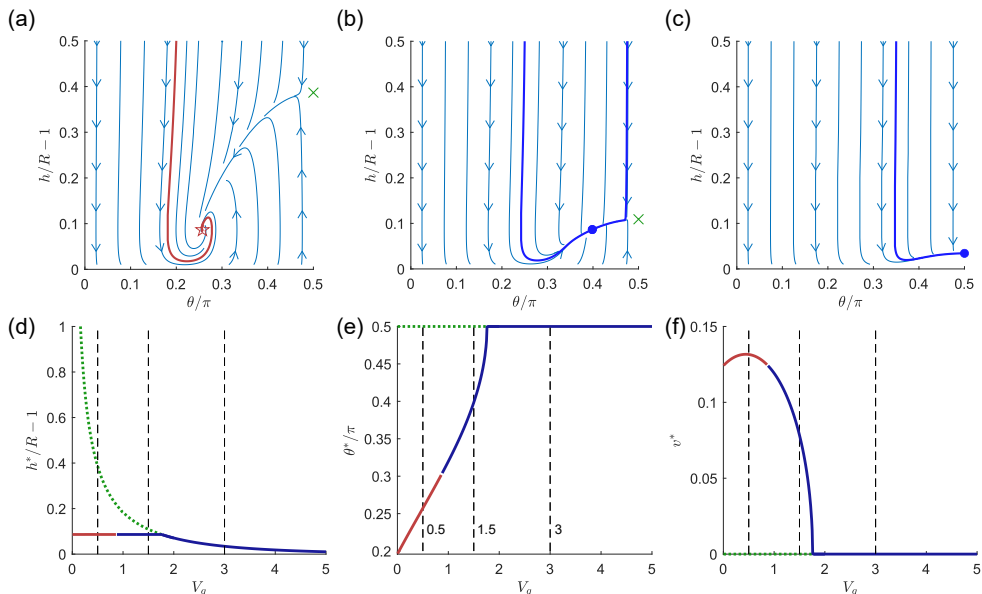


Figure 13: Bifurcation structures of swimming dynamics for a squirmer with $B_1 = 0, B_2 = -1$ (extensile shaker). Top row: (a) $V_g = 0.5$, (b) $V_g = 1.5$, and (c) $V_g = 3$. Bottom row: Dependence of (d) stable height, (e) orientation, and (f) wall-parallel speed on the free space sedimentation speed V_g . Red curves indicate stable spirals and blue curves indicate stable nodes. Green dashed curves indicates saddle nodes.

rheology. For example, biological fluids such as blood and mucus are typically shear-thinning fluids that have profound effects on locomotion of microswimmers. Novel particle–wall interactions in a shear-thinning non-Newtonian fluid have been studied in the context of the rolling of a rotating sphere near a solid wall (Chen *et al.* 2021). For a sphere rolling on the wall, the non-Newtonian shear-thinning rheology can give rise to wall-induced translation opposite to the direction of friction against the wall (Chen *et al.* 2021). Li & Ardekani (2017) studied the effects of non-Newtonian rheology on the interactions between an undulatory swimmer next to a wall. How would non-Newtonian rheology alter the swimming dynamics of a squirmer next to a rigid wall? It would be interesting to investigate the non-Newtonian effects on the bifurcation structures of the swimming dynamics of a squirmer next to a solid wall.

In a porous medium, the interactions between the active swimmers and the complex boundaries are essential to understanding the diffusive transport of active suspensions such as bacteria that transition between states as they run and tumble (Datta *et al.* 2024). Our results show that, under gravity, the squirmer has multiple trajectories between being bound to the wall or escaping from the wall by varying α (the relative propulsion velocity to the sedimenting velocity) and β (the relative strength of the swimming mode to the contractile/extensile mode). For a squirmer sedimenting in a porous medium, each time it encounters an obstacle it can transition between states that we reported here, similar to the transitions of run-and-tumbling bacteria in porous media (Mattingly 2023). It would be interesting to quantify how the effective diffusivity of squirmer sedimenting in a porous medium depends on α and β .

Acknowledgement

The authors acknowledge useful discussions with Bryan Quaife and On Shun Pak. YNY acknowledges support by the National Science Foundation (NSF) under award DMS- 1951600, and of the Flatiron Institute, part of Simons Foundation. HS acknowledges the support of the Natural Sciences and Engineering Research Council of Canada (NSERC), [funding reference number RGPIN-2018-04418]. Cette recherche a été financée par le Conseil de recherches en sciences naturelles et en génie du Canada (CRSNG), [numéro de référence RGPIN-2018-04418].

Declaration of Interests: The authors report no conflict of interest.

REFERENCES

- AHMED, DANIEL, SUKHOV, ALEXANDER, HAURI, DAVID, RODRIGUE, DUBON, MARANTA, GIAN, HARTING, JENS & NELSON, BRADLEY J 2021 Bioinspired acousto-magnetic microswarm robots with upstream motility. *Nature Machine Intelligence* **3** (2), 116–124.
- ALAPAN, YUNUS, BOZUYUK, UGUR, ERKOC, PELIN, KARACAKOL, ALP CAN & SITTI, METIN 2020 Multifunctional surface microrollers for targeted cargo delivery in physiological blood flow. *Science Robotics* **5** (42), eaba5726.
- BERKE, ALLISON P, TURNER, LINDA, BERG, HOWARD C & LAUGA, ERIC 2008 Hydrodynamic attraction of swimming microorganisms by surfaces. *Physical Review Letters* **101** (3), 038102.
- BLAKE, J. R. 1971a A note on the image system for a stokeslet in a no-slip boundary. *Math. Proc. Cambridge Philos. Soc.* **70** (2), 303–310.
- BLAKE, J. R. 1971b A spherical envelope approach to ciliary propulsion. *J. Fluid Mech* **46** (1), 199–208.
- BRADY, JOHN F & BOSSIS, GEORGES 1985 The rheology of concentrated suspensions of spheres in simple shear flow by numerical simulation. *Journal of Fluid mechanics* **155**, 105–129.
- BRENNER, HOWARD 1961 The slow motion of a sphere through a viscous fluid towards a plane surface. *Chemical Engineering Science* **16** (3-4), 242–251.
- CHEN, YE, DEMIR, EBRU, GAO, WEI, YOUNG, Y-N & PAK, ON SHUN 2021 Wall-induced translation of a rotating particle in a shear-thinning fluid. *Journal of Fluid Mechanics* **927**, R2.
- COOLEY, M. D. A. & O'NEILL, M. E. 1969 On the slow motion generated in a viscous fluid by the approach of a sphere to a plane wall or stationary sphere. *Mathematika* **16** (1), 37–49.
- COX, RAYMOND G & BRENNER, HOWARD 1967 The slow motion of a sphere through a viscous fluid towards a plane surface—ii small gap widths, including inertial effects. *Chemical Engineering Science* **22** (12), 1753–1777.
- CROWDY, DARREN G & OR, YIZHAR 2010 Two-dimensional point singularity model of a low-reynolds-number swimmer near a wall. *Physical Review E—Statistical, Nonlinear, and Soft Matter Physics* **81** (3), 036313.
- DATTA, AGNIVA, BETA, CARSTEN & GROSMANN, ROBERT 2024 The random walk of intermittently self-propelled particles. *arXiv preprint arXiv:2406.15277*.
- DRISCOLL, MICHELLE, DELMOTTE, BLAISE, YOUSSEF, MENA, SACANNA, STEFANO, DONEV, ALEKSANDAR & CHAIKIN, PAUL 2017 Unstable fronts and motile structures formed by microrollers. *Nature Physics* **13** (4), 375–379.
- ELGETI, JENS & GOMPPER, GERHARD 2016 Microswimmers near surfaces. *The European Physical Journal Special Topics* **225**, 2333–2352.
- ISHIKAWA, TAKUJI, SIMMONDS, MP & PEDLEY, TIMOTHY J 2006 Hydrodynamic interaction of two swimming model micro-organisms. *Journal of Fluid Mechanics* **568**, 119–160.
- KIM, SANGTAE & KARRILA, SEPPO J 2013 *Microhydrodynamics: principles and selected applications*. Butterworth-Heinemann.
- KUHR, JAN-TIMM, RÜHLE, FELIX & STARK, HOLGER 2019 Collective dynamics in a monolayer of squirmers confined to a boundary by gravity. *Soft Matter* **15** (28), 5685–5694.
- LI, GAOJIN & ARDEKANI, AREZOO M 2017 Near wall motion of undulatory swimmers in non-newtonian fluids. *European Journal of Computational Mechanics* **26** (1-2), 44–60.
- LI, GUANGLAI & TANG, JAY X 2009 Accumulation of microswimmers near a surface mediated by collision and rotational brownian motion. *Physical Review Letters* **103** (7), 078101.
- LI, GAO-JIN & ARDEKANI, AREZOO M 2014 Hydrodynamic interaction of microswimmers near a wall. *Physical Review E* **90** (1), 013010.

- LIGHTHILL, M. J. 1952 On the squirming motion of nearly spherical deformable bodies through liquids at very small Reynolds numbers. *Communications on Pure and Applied Mathematics* **5** (2), 109–118.
- LINTUVUORI, JUHO S, BROWN, AIDAN T, STRATFORD, KEVIN & MARENUZZO, DAVIDE 2016 Hydrodynamic oscillations and variable swimming speed in squirmers close to repulsive walls. *Soft Matter* **12** (38), 7959–7968.
- MATTINGLY, HENRY 2023 Bacterial diffusion in disordered media, by forgetting the media. *arXiv preprint arXiv:2311.10612* .
- OR, YIZHAR & MURRAY, RICHARD M 2009 Dynamics and stability of a class of low reynolds number swimmers near a wall. *Physical Review E—Statistical, Nonlinear, and Soft Matter Physics* **79** (4), 045302.
- PAPAVASSILIOU, DARIO & ALEXANDER, GARETH P 2017 Exact solutions for hydrodynamic interactions of two squirming spheres. *Journal of Fluid Mechanics* **813**, 618–646.
- POZRIKIDIS, CONSTANTINE 1992 *Boundary integral and singularity methods for linearized viscous flow*. Cambridge University Press.
- RÜHLE, FELIX, BLASCHKE, JOHANNES, KUHR, JAN-TIMM & STARK, HOLGER 2018 Gravity-induced dynamics of a squirmer microswimmer in wall proximity. *New Journal of Physics* **20** (2), 025003.
- SHUM, HENRY, GAFFNEY, EAMONN A & SMITH, DAVID J 2010 Modelling bacterial behaviour close to a no-slip plane boundary: the influence of bacterial geometry. *Proceedings of the Royal Society A: Mathematical, Physical and Engineering Sciences* **466** (2118), 1725–1748.
- SING, CHARLES E, SCHMID, LOTHAR, SCHNEIDER, MATTHIAS F, FRANKE, THOMAS & ALEXANDER-KATZ, ALFREDO 2010 Controlled surface-induced flows from the motion of self-assembled colloidal walkers. *Proceedings of the National Academy of Sciences* **107** (2), 535–540.
- SPAGNOLIE, SAVERIO E & LAUGA, ERIC 2012 Hydrodynamics of self-propulsion near a boundary: predictions and accuracy of far-field approximations. *Journal of Fluid Mechanics* **700**, 105–147.
- STIMSON, MARGARET & JEFFERY, GEORGE BARKER 1926 The motion of two spheres in a viscous fluid. *Proceedings of the Royal Society of London. Series A, Containing Papers of a Mathematical and Physical Character* **111** (757), 110–116.
- TAKAGI, DAISUKE, PALACCI, JÉRÉMIE, BRAUNSCHWEIG, ADAM B, SHELLEY, MICHAEL J & ZHANG, JUN 2014 Hydrodynamic capture of microswimmers into sphere-bound orbits. *Soft Matter* **10** (11), 1784–1789.
- THÉRY, A, MAAß, CC & LAUGA, E 2023 Hydrodynamic interactions between squirmers near walls: far-field dynamics and near-field cluster stability. *Royal Society Open Science* **10** (6), 230223.
- TIERNO, PIETRO, GOLESTANIAN, RAMIN, PAGONABARRAGA, IGNACIO & SAGUÉS, FRANCESC 2008 Controlled swimming in confined fluids of magnetically actuated colloidal rotors. *Physical review letters* **101** (21), 218304.
- WÜRGER, ALOIS 2016 Hydrodynamic boundary effects on thermophoresis of confined colloids. *Physical Review Letters* **116** (13), 138302.
- YARIV, EHUD 2016 Thermophoresis of confined colloids in the near-contact limit. *Physical Review Fluids* **1** (2), 022101.